NASA/TM—2017-219551

Reconfigurable Wideband Circularly Polarized Stacked Square Patch Antenna for Cognitive Radios

Miguel A. Barbosa Kortright
Universities Space Research Association, Glenn Research Center, Cleveland, Ohio

Seth W. Waldstein and Rainee N. Simons
Glenn Research Center, Cleveland, Ohio

August 2017

NASA STI Program . . . in Profile

Since its founding, NASA has been dedicated to the advancement of aeronautics and space science. The NASA Scientific and Technical Information (STI) Program plays a key part in helping NASA maintain this important role.

The NASA STI Program operates under the auspices of the Agency Chief Information Officer. It collects, organizes, provides for archiving, and disseminates NASA's STI. The NASA STI Program provides access to the NASA Technical Report Server—Registered (NTRS Reg) and NASA Technical Report Server—Public (NTRS) thus providing one of the largest collections of aeronautical and space science STI in the world. Results are published in both non-NASA channels and by NASA in the NASA STI Report Series, which includes the following report types:

- TECHNICAL PUBLICATION. Reports of completed research or a major significant phase of research that present the results of NASA programs and include extensive data or theoretical analysis. Includes compilations of significant scientific and technical data and information deemed to be of continuing reference value. NASA counter-part of peer-reviewed formal professional papers, but has less stringent limitations on manuscript length and extent of graphic presentations.

- TECHNICAL MEMORANDUM. Scientific and technical findings that are preliminary or of specialized interest, e.g., "quick-release" reports, working papers, and bibliographies that contain minimal annotation. Does not contain extensive analysis.

- CONTRACTOR REPORT. Scientific and technical findings by NASA-sponsored contractors and grantees.

- CONFERENCE PUBLICATION. Collected papers from scientific and technical conferences, symposia, seminars, or other meetings sponsored or co-sponsored by NASA.

- SPECIAL PUBLICATION. Scientific, technical, or historical information from NASA programs, projects, and missions, often concerned with subjects having substantial public interest.

- TECHNICAL TRANSLATION. English-language translations of foreign scientific and technical material pertinent to NASA's mission.

For more information about the NASA STI program, see the following:

- Access the NASA STI program home page at http://www.sti.nasa.gov

- E-mail your question to help@sti.nasa.gov

- Fax your question to the NASA STI Information Desk at 757-864-6500

- Telephone the NASA STI Information Desk at 757-864-9658

- Write to:
  NASA STI Program
  Mail Stop 148
  NASA Langley Research Center
  Hampton, VA 23681-2199

NASA/TM—2017-219551

Reconfigurable Wideband Circularly Polarized Stacked Square Patch Antenna for Cognitive Radios

Miguel A. Barbosa Kortright
Universities Space Research Association, Glenn Research Center, Cleveland, Ohio

Seth W. Waldstein and Rainee N. Simons
Glenn Research Center, Cleveland, Ohio

National Aeronautics and
Space Administration

Glenn Research Center
Cleveland, Ohio 44135

August 2017

Acknowledgments

Miguel A. Barbosa Kortright acknowledges Mr. Seth W. Waldstein for his help in the photolithographic fabrication of the antenna elements, NASA Mentor, Dr. Rainee N. Simons for his expert input during the design process, Dale Force with the material procurements, and NASA Glenn for the internship opportunity.

Supplementary Notes

The figures are archived under E-19403.

This report contains preliminary findings, subject to revision as analysis proceeds.

Level of Review: This material has been technically reviewed by technical management.

Available from

NASA STI Program
Mail Stop 148
NASA Langley Research Center
Hampton, VA 23681-2199

National Technical Information Service
5285 Port Royal Road
Springfield, VA 22161
703-605-6000

This report is available in electronic form at http://www.sti.nasa.gov/ and http://ntrs.nasa.gov/

Reconfigurable Wideband Circularly Polarized Stacked Square Patch Antenna for Cognitive Radios

Miguel A. Barbosa Kortright*
Universities Space Research Association
Glenn Research Center
Cleveland, Ohio 44135

Seth W. Waldstein† and Rainee N. Simons
National Aeronautics and Space Administration
Glenn Research Center
Cleveland, Ohio 44135

Abstract

An almost square patch, a square patch and a stacked square patch with corner truncation for circular polarization (CP) are researched and developed at X-band for cognitive radios. Experimental results indicate, first, that the impedance bandwidth of a CP almost square patch fed from the edge by a 50 ohm line is 1.70 percent and second, that of a CP square patch fed from the ground plane side by a surface launch connector is 1.87 percent. Third, the impedance bandwidth of a CP stacked square patch fed by a surface launch connector is 2.22 percent. The measured center frequency for the CP square patch fed by a surface launch connector without and with an identical stacked patch is 8.45 and 8.1017 GHz, respectively. By stacking a patch, separated by a fixed air gap of 0.254 mm, the center frequency is observed to shift by as much as 348.3 MHz. The shift in the center frequency can be exploited to reconfigure the operating frequency by mechanically increasing the air gap. The results indicate that a tuning bandwidth of about 100 MHz can be achieved when the distance of separation between the driven patch and the stacked patch is increased from its initial setting of 0.254 to 1.016 mm.

Introduction

One of the greatest design challenges for cognitive radio antennas is creating wideband elements. Software defined radio (SDR) is seen as an enabling technology for cognitive radio, which offers much promise to increase spectrum usage efficiencies to users in a wide variety of applications, including space communications (Ref. 1). In the context of space communications, NASA's Near Earth Network (NEN) is interested in the X-Band frequencies (8.0 to 8.5 GHz) to establish space-to-Earth downlinks for science spacecraft using cognitive radios. The use of this frequency band can be achieved through the reconfigurable nature of cognitive radios. Reconfiguration in cognitive radios is achieved through the use of software modules to adapt the radio's internal states to statistical variations in the incoming RF stimuli (Refs. 2 and 3). The physical layer of the cognitive radio (antennas, conversion modules, etc.) is not often associated with the reconfigurable capabilities of the cognitive radio. In this paper, the design of wideband circularly polarized (CP) patch antennas for frequency reconfiguration in the physical layer of cognitive radios are studied and reported at X-Band frequencies.

Due to their lightweight, low cost, and ease of fabrication, patch antennas are attractive for wireless communications. The drawback for these antennas is their narrow bandwidth (Ref. 4). Two designs were researched and fabricated to improve bandwidth and demonstrate frequency reconfiguration at the physical level for cognitive devices: (1) A microstrip almost square patch antenna with corner truncation for CP, fed through the edge with a 50 ohm microstrip line; (2) A microstrip square patch antenna with corner truncation for CP, fed from the ground plane side with a surface launch connector. These designs were studied as both standalone and stacked geometries. A stacked square patch with corners truncated for CP, fed from the edge by a 50 ohm line and having an impedance bandwidth of 1.3 GHz (11.2 to 12.5 GHz) has been demonstrated in Reference 5. However, this geometry offers considerable challenges in the realization of large arrays since it would require the antennas and feed networks to be in a planar configuration (Ref. 6). To address this issue, the microstrip square patch fed from the ground plane side with a surface launch connector was investigated in greater detail. This type of feeding arangement has several advantages: (1) It can be configured into a large planar array, (2) It allows for hybrid integration of phase-shifters and solid-state power amplifiers (SSPA) located either on an orthogonal substrate or on a multi-layer substrate, (3) It can be scaled to higher frequencies of interest to NASA missions.

Reconfiguration of the physical layer of the cognitive radio becomes feasable when a stacked antenna is added into the system. The stacked antenna element creates the potential of a mechanically tunable system, expanding the usable antenna net impedance bandwidth and operating center frequencies for use in spectrum sensing and transmission. The mechanical tunning of the stacked antenna is achieved manually. Furthermore, the tuning can be done electronically through the addition of an external mechanism, such as RF-MEMS circuitry.

*Intern with Universities Space Research Association Program, affiliated with University of Puerto Rico
†NASA Intern with Lewis Educational and Research Collaborative Internship Project (LERCIP), affiliated with University of Cincinnati

Microstrip Patch Antenna Design and Simulation

Standalone Antennas

The antennas were designed and simulated using CST Microwave Studios 2010 and its built in material library (Ref. 7). Roger's Corporation's RO3003 (ε_r = 3.0, h = 0.508 mm, g = 60 mm) substrate with half-ounce cooper cladding (t = 0.01778 mm) was considered for the antennas.

The lengths and widths (L_1, W_1, L_2, and W_2) and corner truncations (C_1 and C_2) for the antennas in Figure 1 were calculated with equations from Reference 8. The Trust Region Algorithm was utilized in CST to optimize the antenna dimensions in order to get the best possible results for the design frequency of 8.4 GHz. The dimension G represents the width of the 50 ohm transmission line that is used to feed the almost square patch antenna and is calculated using ADS's Line Calc. The dimension D represents the final optimized position with respect to the center of the square patch antenna in which the surface launch connector pin is introduced from the ground plane side of the substrate. The dimensions C_1 and C_2 represent corner truncations for circular polarization. Table I summarizes the antenna dimensions.

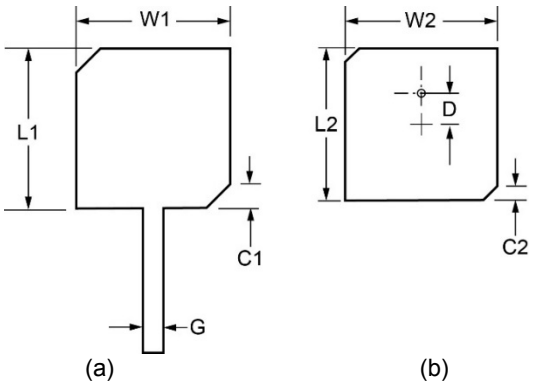

Figure 1.—Standalone antenna geometry. (a) Almost square patch with 50 ohms microstrip feed. (b) Square patch excited from the ground plane side by a surface launch connector.

TABLE I.—DIMENSIONS OF THE STANDALONE ANTENNAS (mm)

Dimensions	
L_1	10.337
W_1	10
C_1	1.487
G	1.277
L_2	9.856
W_2	9.856
C_2	0.873
D	2

There is not much information on the exact location of an efficient feed point for the surface launch type of excitation in the open literature for X-Band applications. It is reported in Reference 9 that at 2.48 GHz a good feed point could be 55 percent towards the edge, from the center point of the antenna. A study reported in Reference 10 indicated that the best input VSWR for a patch at 3.103 GHz was obtained with a feed point 64 percent towards the edge, from the center point of the antenna. Consequently, in the initial design the position of the feed point was placed between 45 and 55 percent towards the edge, from the center point of the antenna. The final CST optimized position represented a move of 40.4 percent towards the edge, from the center point of the antenna. The simulation took into consideration the surface launch connector pin radius and dielectric radius of 0.254 and 1.016 mm, respectively. The ground plane corresponding to the cross sectional area of the connector dielectric is removed in the simulation to match the fabricated geometry.

Stacked Antenna

The stacked square patch antenna geometry consists of an identical patch antenna without a ground plane stacked on top of a driven patch antenna, as illustrated in Figure 2. The driven patch and the stacked patch have identical substrate properties. There is a minimum air gap of 0.254 mm between the driven patch and stacked patch due to the solder bump that was created during the assembly process to hold the coaxial connector pin in place.

It is worth mentioning that by stacking a patch on an almost square patch with a 50 ohm feed would also impact the feed line propagation characteristics (Fig. 1(a)). This is because the over layed stacked dielectric substrate now appears as a superstrate for the feed line. Such an arrangement would necessitate reconfiguring the 50 ohm feed line and the patch antenna characteristics simultaneously, which would render the stacked antenna design far more complicated. Therefore, the stacked geometry was only pursued for the standalone square patch, fed from the ground plane side by a surface launch connector (Fig. 1(b)).

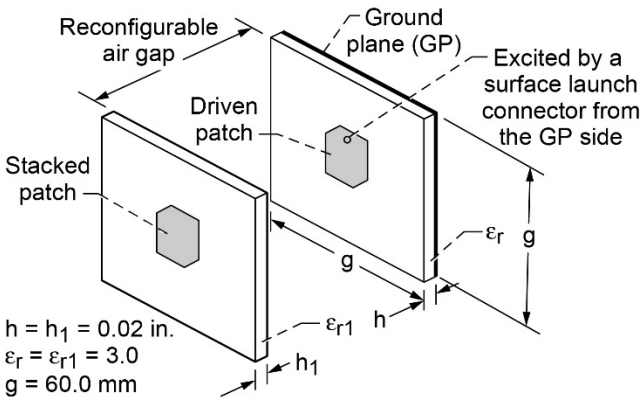

Figure 2.—Stacked square patch antenna geometry with identical driven and stacked patches.

Simulated Results—Center Frequency and Impedance Bandwidth

Figures 3(a) and (b) shows the simulated S_{11} for the two standalone geometries (Fig. 1). The simulated results show that the center frequency (f_0) for both standalone cases are similar and close to the design frequency of 8.4 GHz. The return loss magnitude at f_0 for the square patch is better than the almost square patch by approximately 3 dB. In addition, the square patch had a better impedance bandwidth (BW) than the standalone almost square patch by 0.24 percent. Table II presents a summary of the information extracted from Figures 3(a) and (b).

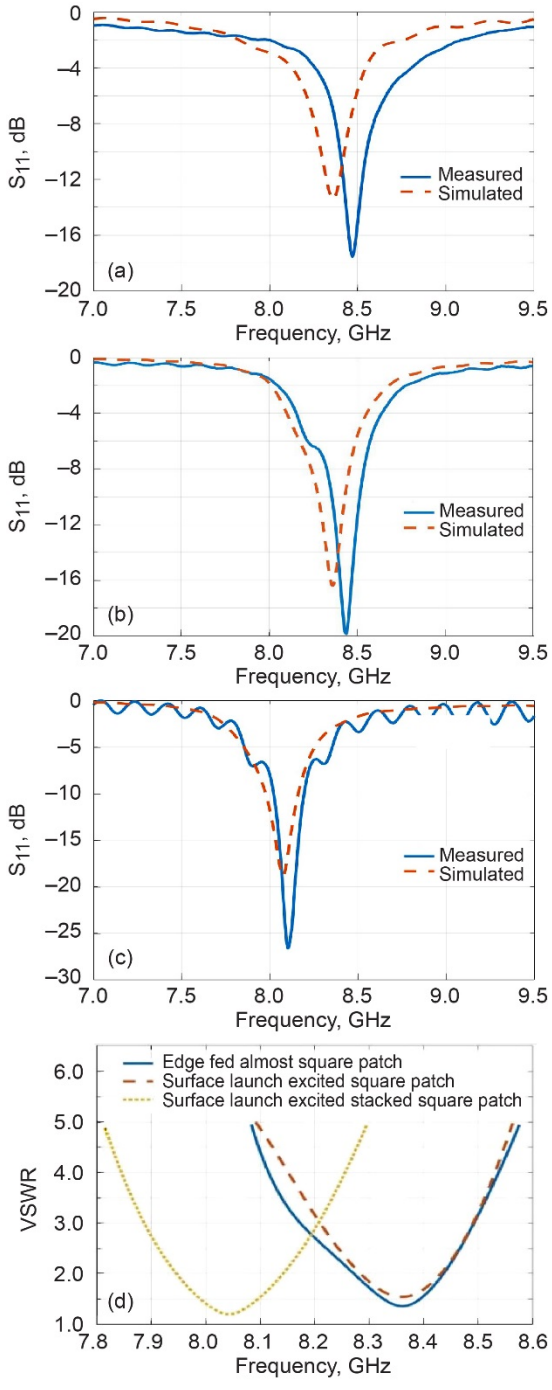

Figure 3.—Simulated and Experimental S_{11}: (a) Almost square patch, (b) Square patch, (c) Stacked square patch. Simulated VSWR: (d) All three cases.

TABLE II.—SUMMARY OF CST SIMULATED S_{11} AND BANDWIDTH DATA FOR STANDALONE ALMOST SQUARE PATCH AND SQUARE PATCH ANTENNAS

	f_0 (GHz)	Return loss (dB)	f_L (GHz)	f_H (GHz)	BW = f_H - f_L (MHz)	BW/f_0 (%)
Standalone almost square patch, fed from edge	8.356	13.460	8.2888	8.4203	131.5	1.57
Standalone square patch, fed through back with surface launch connector	8.364	16.375	8.2797	8.4314	151.7	1.81

TABLE III.—SUMMARY OF CST SIMULATED S_{11} AND BANDWIDTH DATA FOR STACKED SQUARE PATCH ANTENNA FOR A FIXED AIR GAP OF 0.254 mm

	f_0 (GHz)	Return loss (dB)	f_L (GHz)	f_H (GHz)	BW = f_H - f_L (MHz)	BW/f_0 (%)
Stacked square patch, fed through back with surface launch connector	8.076	18.869	7.9755	8.1625	187	2.31

Figure 3(c) shows the simulated S_{11} for the stacked square patch antenna (Fig. 2). The simulated center frequency for the square patch excited by a surface launch connector without and with a stacked patch is 8.364 and 8.076 GHz, respectively. Thus by stacking a patch, separated by a fixed air gap of 0.254 mm, the center frequency is observed to shift by as much as 288 MHz (3.44 percent). In addition, the impedance bandwidth increases by 0.5 percent. It is worth noting that by increasing the air gap to 1.016 mm in increments of 0.254 mm, the center frequency of the stacked system moved closer to the center frequency of the standalone antenna. The effects of the air gap are discussed in a further section. Table III summarizes the data extracted from Figure 3(c). Figure 3(d) shows the VSWR for all three cases and is observed to be under two, which is desirable.

Simulated Results—Radiation Pattern

The starting ground plane size was 60×60 mm. When varying the plane size by 30 mm, incrementialy and decrementialy, the directivity and realized gain improve, while the angular width varies. The best directivity and realized gain was achieved when the ground plane size was 30×30 mm, therefore the radiation patterns were simulated with that ground plane size.

Figures 4(a) to (c) shows the simulated radiation patterns in Cartesian coordinates in the two principal planes for the three antenna geometries discussed earlier. The inset in Figure 4(a) shows the reference cartesian coordinate system.

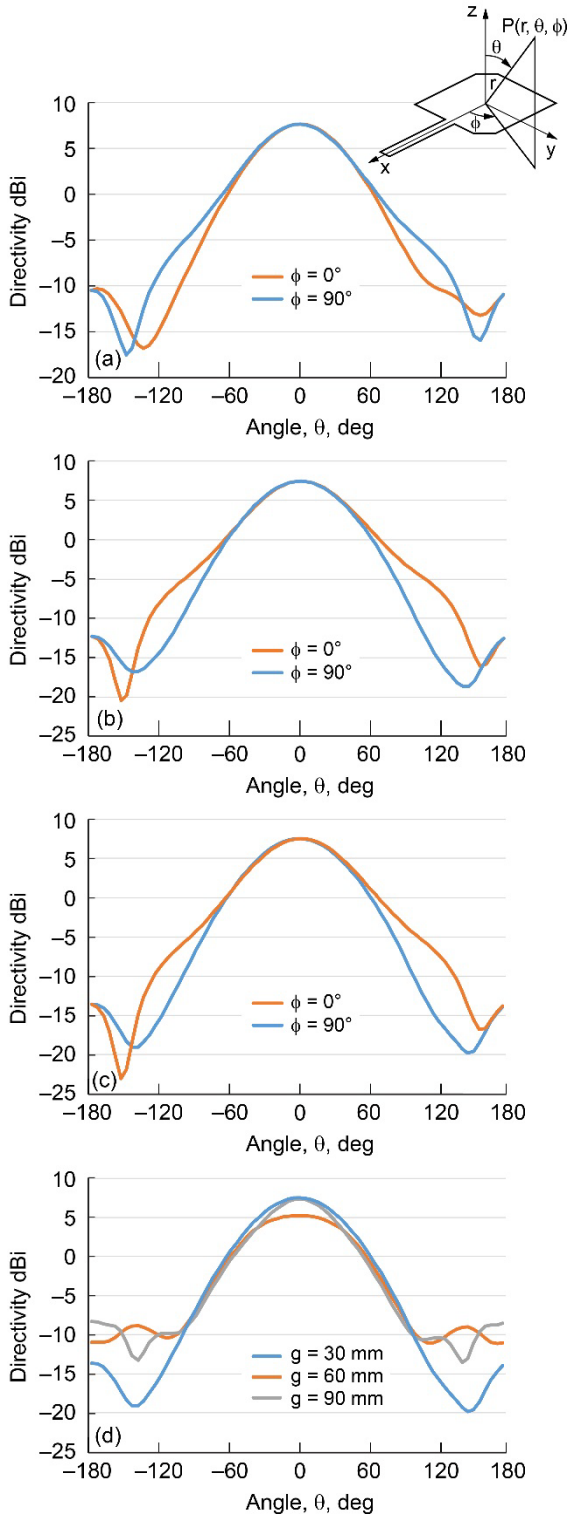

Figure 4.—Simulated Radiation Pattern: (a) Almost square patch, (b) Square patch, (c) Stacked square patch, (d) Stacked square patch when ground plane dimensions are varied.

Figure 4(d) shows the effect of ground plane size on the radiation pattern of the stacked square patch antenna. Tables IV and V present a summary of the antenna characteristics that were extracted from Figures 4(a) to (c). Table VI presents a summary of the effects of the ground plane size on the stacked square patch radiation pattern.

The change that occurs in the 3 dB Angular Width of the Standalone Almost Square Patch when we study both Phi = 0° and Phi = 90° is due to the fact that the width and length of the designed antenna are not the same. When comparing the Standalone Square Patch in the same context, there is no significant change in the antenna characteristics due to the dimensions being equal. When comparing the Standalone and Stacked Square Patches, we see a decrease in 3 dB Angular Width due to an increase in gain.

TABLE IV.—SUMMARY OF CST SIMULATED RADIATION PATTERN WITH PHI EQUAL TO NINETY

	Directivity (dBi)	Realized gain (dB)	3 dB angular width (deg.)
Standalone Almost Square Patch, Fed From Edge	7.65	6.7	76.4
Standalone Square Patch, Fed Through Back With Surface Launch Connector	7.45	6.75	76.6
Stacked Square Patch, Fed Through Back With Surface Launch Connector	7.53	7.1	76.1

TABLE V.—SUMMARY OF CST SIMULATED RADIATION PATTERN WITH PHI EQUAL TO ZERO

	Directivity (dBi)	Realized gain (dB)	3 dB angular width (deg.)
Standalone almost square patch, fed from edge	7.65	6.7	75
Standalone square patch, fed through back with surface launch connector	7.45	6.75	77
Stacked square patch, fed through back with surface launch connector	7.53	7.1	76.7

TABLE VI.—SUMMARY OF CST SIMULATED GROUND PLANE VARIATION FOR STACKED SQUARE PATCH AND PHI EQUAL TO NINETY

	Directivity (dBi)	Realized gain (dB)	3 dB angular width (deg.)
Ground plane size 30×30 mm	7.53	7.1	76.1
Ground plane size 60×60 mm	5.25	4.81	92.5
Ground plane size 90×90 mm	7.36	6.92	64.6

Simulated Results—Polarization

The corner truncations shown in Figure 1 resulted in an antenna that is left hand circularly polarized (LHCP). Truncating the opposite two corners would result in an antenna that is right hand circularly polarized (RHCP).

Figure 5 illustrates the simulated surface currents at different phases for the Square Patch antenna, with respect to the feed side of the element. Starting at a phase of 0°, the surface currents exhibit a starting position. As the phase increments in steps of 90°, a counter clock wise pattern defines the currents. When the phase reaches 360° the surface currents are in the same position as when the phase equaled 0°, thus proving a circular cycle and LHCP through simulation.

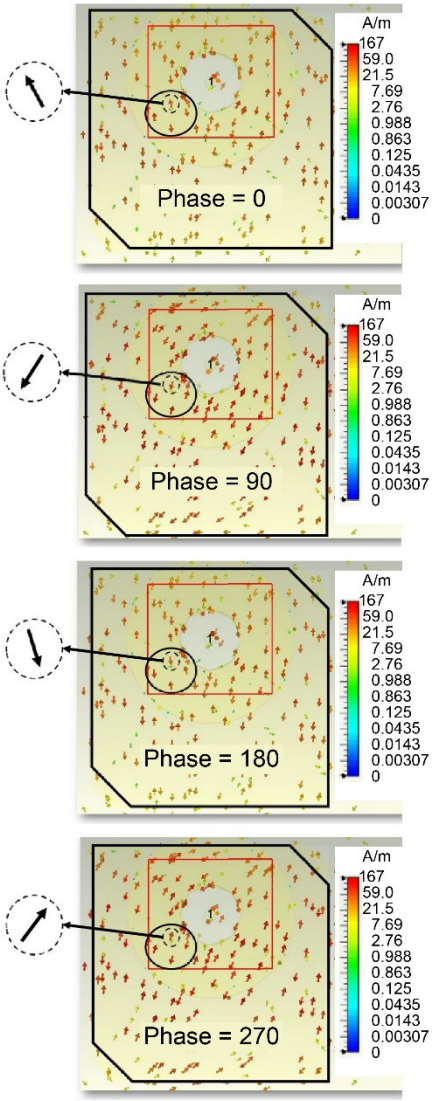

Figure 5.—(a) Surface curretns with counter clockwise pattern as observed from the feed side.

Microstrip Patch Antenna Fabrication and Characterization

Fabrication

The standalone patch antennas and the stacked patch antenna discussed above were fabricated using a photolithographic process. The two fabricated standalone antennas are shown in Figure 6(a) and (b), respectively. The antenna dimensions are identical to the simulated dimensions presented in Table I. In the case of the antenna shown in Figure 6(b) a surface launch connector was used to excite the patch from the ground plane side. The center pin of the

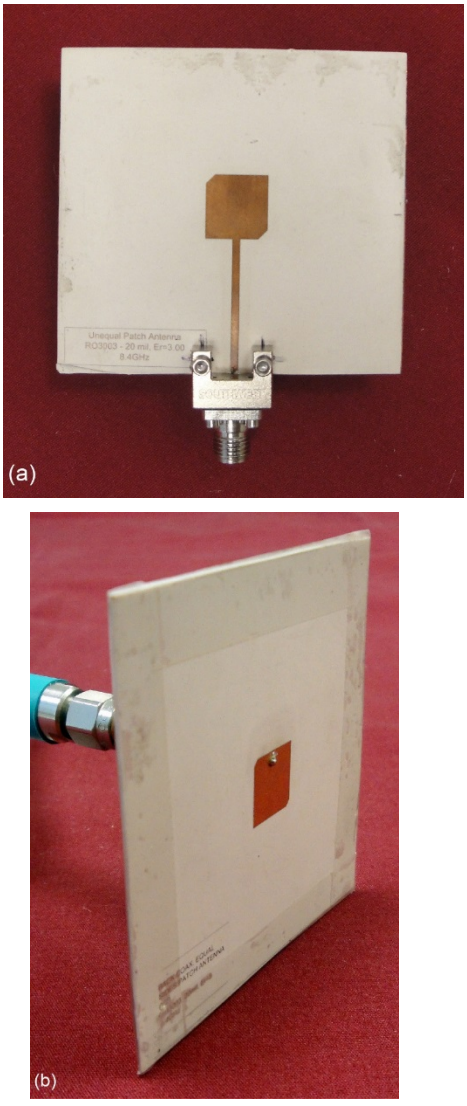

Figure 6.—(a) Fabricated standalone almost square patch fed through the edge with a 50 ohm microstrip transmission line. (b) Fabricated standalone square patch fed through the ground plane side by a surface launch connector.

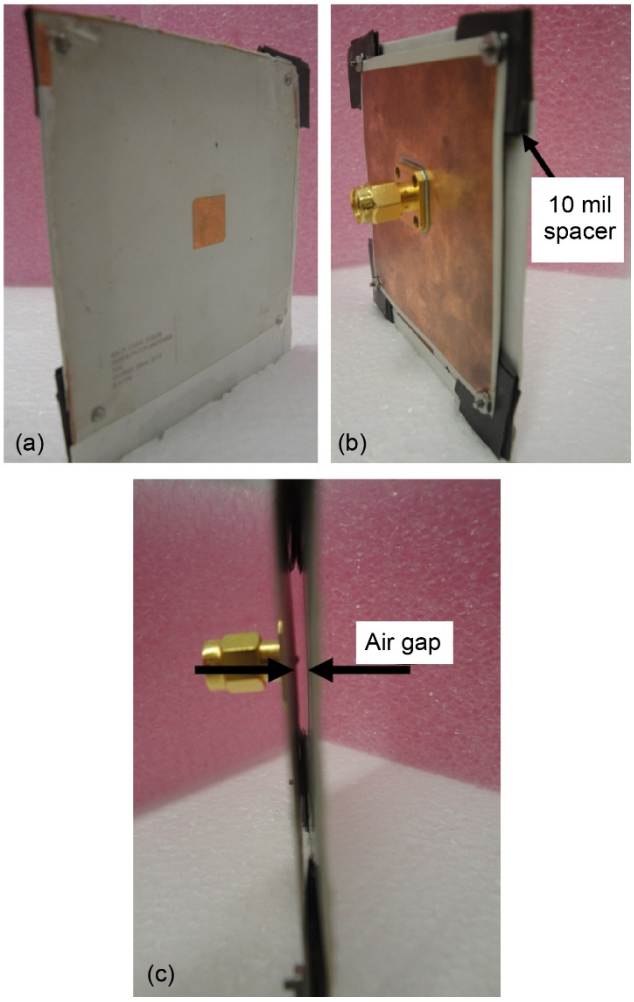

Figure 7.—(a) Front view of fabricated stacked square patch showing an identical stacked patch. (b) Back view of the fabricated stacked square patch antenna showing the feeding arrangement through the ground plane side of the driven patch by a surface launch connector. (c) The driven patch and the stacked patch are separated by a minimum air gap of 0.254 mm.

connector was located approximately 40 percent towards the edge, from the center of the patch as illustrated in Figure 1(b). The diameter of the center pin and the exposed portion of the coaxial dielectric of the connector are approximately 0.508 and 2.54 mm, respectively. The fabricated stacked square patch antenna is shown in Figures 7(a) to (c).

Characterization

The test setup for characterizing the return loss of the standalone and the stacked patch antennas consisted of an Agilent Technologies E8363B Vector Network Analyzer with phase stable measurement cables. A small anechoic chamber (Fig. 8) was constructed utilizing absorbent paneling in order to transmit a signal from a reference LHCP X-Band spiral antenna and capture it with the fabricated elements. A Spectrum analyzer was used to validate reception and experimentally prove LHCP. The measured S_{11} for the two standalone antennas and the stacked antenna are superimposed on the simulated results in Figures 3(a) to (c), respectively. The experimental data extracted from these figures are summarized in Table VII.

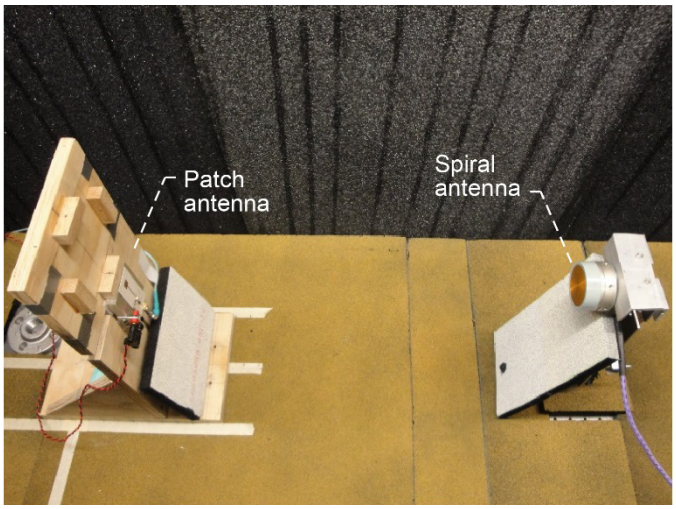

Figure 8.—Anechoic chamber with X-Band LHCP reference spiral antenna and almost square patch antenna.

TABLE VIII.—SUMMARY OF EXPERIMENTAL DATA FOR THE STANDALONE AND STACKED PATCH ANTENNAS. THE AIR GAP IS 0.254 MM IN THE CASE OF STACKED PATCHES

	f_0 (GHz)	Return loss (dB)	f_L (GHz)	f_H (GHz)	BW = $f_H - f_L$ (MHz)	BW/f_0 (%)
Standalone almost square patch, fed from edge	8.46	17.5402	8.385	8.529	144	1.7
Standalone square patch, fed through back with surface launch connector	8.45	19.7545	8.3675	8.5255	158	1.87
Stacked square patch, fed through back with surface launch connector	8.1017	25.7	8.0204	8.2005	180.1	2.22

Experiments show that the impedance bandwidth of the standalone antenna fed from the edge by a 50 ohm line is 1.70 percent and that of the antenna fed from the ground plane side by a surface launch connector is 1.87 percent. In addition, the impedance bandwidth of the stacked square patch fed from the ground plane side by a surface launch connector is 2.22 percent. These results indicate that the surface launch type of excitation results in larger impedance bandwidth when compared to edge feeding. Furthermore, the measured center frequency for the square patch excited by a surface launch connector without and with a stacked patch is 8.45 and 8.1017 GHz, respectively. Thus by stacking a patch, separated by a fixed air gap of 0.254 mm, the center frequency is observed to shift by as much as 348.3 MHz (4.12 percent). Moreover, the simulated and measured results are within 1.24 percent in all three cases and therefore, considered to be in excellent agreement. The experimental validation of the observed simulated frequency shift discussed earlier strengthens the case for the feasibility in using an external mechanism to electronically reconfigure the stacked antennas in the physical layer of a cognitive radio. The fixed air gap was manually moved in increments of 0.254 mm and was in agreement with the behavior discussed in the simulated results.

Antenna Frequency Reconfiguration in Cognitive Radios

The shift in the center frequency when a stacked element is added to the standalone element, as discussed above, would enable the electronic reconfiguration of the operating frequency in the physical layer of the cognitive radio to be plausible by way of an external mechanism. The spectrum sensing portion of the cognitive radio would be used initially to identify spectrum holes in the designated band of frequencies and then the software would reconfigure the internal states of the radio to become functional in the available spectrum. The external mechanism would reconfigure the antenna geometry at the physical level of the cognitive radio to be able to transmit at the available spectrum.

Figure 9(a) and (b) show the simulated and experimental graphs for the effect of the air gap variation. Table VIII contains a summary of the air gap effect. CST simulations showed that by increasing the air gap from its initial value of 0.254 mm to four times the initial value (1.016 mm), the central frequency of the stacked patch can be reconfigured from 8.076 to 8.130 GHz. Beyond 1.016 mm, the driven patch and the stacked patch begin to decouple and the air gap has no significant influence on the central frequency. Taking the above simulated central frequency shift and the air gap dimensions into account, the central frequency sensitivity of the system is on the order of 7.06 MHz per 100 microns of change in the air gap dimension.

Furthermore, manually increasing the air gap from its initial value of 0.254 mm to four times the initial value (1.016 mm), the central frequency of the stacked patch can be reconfigured from 8.1017 to 8.2017 GHz. The experimental central frequency shift of the system is on the order of 13.12 MHz per 100 microns of change in the air gap dimension.

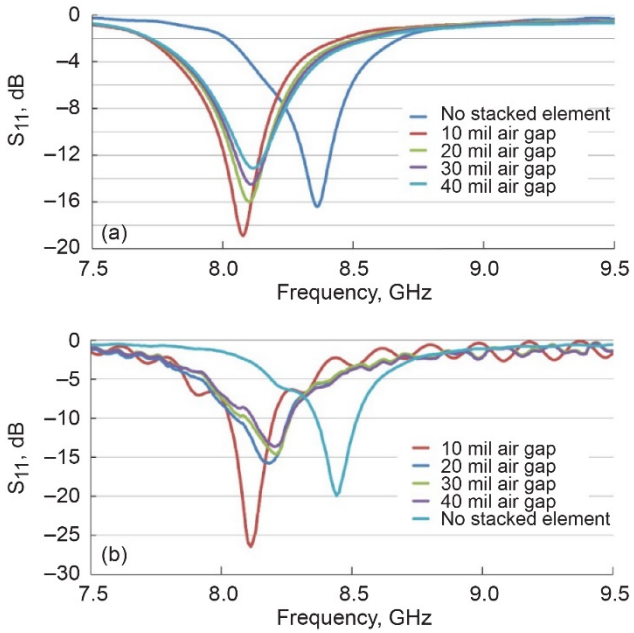

Figure 9.—(a) Simulated air gap variation. (b) Experimental air gap variation.

TABLE VIII.—SUMMARY OF SIMULATED AND EXPERIMENTAL DATA FOR AIR GAP VARIATION

	Air gap (mil)	f_0 (GHz)	Return loss (dB)	BW = f_H- f_L (MHz)	BW/f_0 (%)
Simulated stacked SP reconfiguration	∞	8.364	16.375	151.7	1.81
	40	8.13	13.10	165	2.02
	30	8.11	14.49	170	2.09
	20	8.10	15.97	180	2.21
	10	8.076	18.85	180	2.23
Measured stacked SP reconfiguration	∞	8.45	19.7545	158	1.87
	40	8.2017	13.68	140	1.70
	30	8.195	14.56	165	2.01
	20	8.18	15.81	205	2.51
	10	8.1017	25.7	180.1	2.22

Future Work

Frequency Reconfiguration With MEMS Devices

The rate of change and the precision with which the air gap dimensions can be reconfigured are dependent on the capabilities of the external tuning mechanism. Electrostatically actuated MEMS devices (Refs. 11 and 12), electro-active polymers/shape memory alloy actuators (Ref. 13), magnetic actuators (Ref. 14), and displacement multipliers (Ref. 15) when integrated with printed antennas have been demonstrated as a viable technology to reconfigure the antenna characteristics. However, this topic will be investigated in greater detail and results will be presented in a future paper.

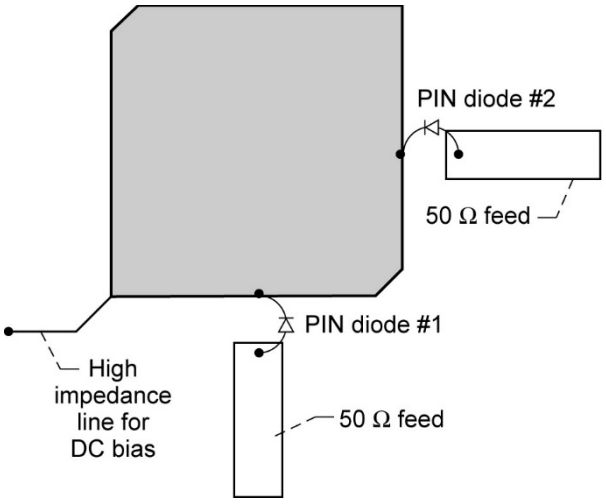

Figure 10.—A square patch excited by two orthogonal microstrip feed lines, which are coupled by two PIN diode switches for switching between LHCP and RHCP. The PIN diode switches are independently controllable.

Polarization Reconfiguration With Semiconductor Devices

A scheme to implement polarization reconfigurability of a CP square patch antenna is illustrated in Figure 7. The two orthogonal feeds are coupled to the patch via two PIN diodes, which can be biased independently. In the arrangement shown, when PIN diode #1 is turned ON and PIN diode #2 is in the OFF state, the antenna is similar to the patch antenna illustrated in Figure 1(a). The antenna radiates a LHCP signal. When PIN diode #1 is turned OFF and PIN diode #2 is turned ON, the antenna radiates a RHCP signal. Polarization reconfiguration would be useful in a cognitive radio because it would enable data transmission in both LHCP and RHCP, which would further expand the capabilities of the cognitive radio.

Conclusions

The simulated and measured results indicate that the impedance bandwidth of the CP square patch antenna excited from the ground plane side by a surface launch connector is superior to the case when excited from the edge by a 50 ohm line. In addition, the impedance bandwidth improves further when an identical patch is stacked above the driven patch. Furthermore, the center frequency shifts in the case of a CP stacked patch geometry. The shift in center frequency can be exploited in a cognitive radio to reconfigure the operating frequency in the presence of interference. The above effort can be extended to NASA's NEN Ka-Band (25.25 to 27.5 GHz) frequencies.

The details on the Solid State Power Amplifier that will be used with the above patch antennas in a cognitive radio can be found in a companion NASA/TM—2017-219552 entitled "Multiband Reconfigurable Harmonically Tuned GaN SSPA for Cognitive Radios," September 2017.

References

1. P.S. Hall, P. Gardner, and A., Faraone, "Antenna Requirements for Software Defined and Cognitive Radios," *Proc. IEEE*, vol. 100, no. 7, pp. 2262–2270, July 2012.
2. J. Mitola III and G.Q. Maguire, Jr., "Cognitive Radio: Making Software Radios More Personal," *IEEE Personal Communications*, vol. 6, no. 4, pp. 13–18, August 1999.
3. S. Haykin, "Cognitive Radio: Brain-Empowered Wireless Communications," *IEEE Journal on Selected Areas in communications*, vol. 23, no. 2, pp. 201–220, February 2005.
4. K. Kiminami, A. Hirata, and T. Shiozawa, "Double-Sided Printed Bow-Tie Antenna for UWB Communications," *IEEE Antennas and Wireless Propagation Letters*, vol. 3, pp. 152–153, 2004.
5. W. Choi, C. Pyo, and J. Choi, "Broadband Circularly Polarized Corner-truncated Square Patch Array Antenna," 2002 *IEEE Antennas and Propagation Society Inter Symp Dig*., vol. 2, pp. 220–223, San Antonio, Tx, 16–21 June 2002.
6. A.R. Weily and N. Nikolic, "Circularly Polarized Stacked Patch Antenna With Perpendicular Feed Substrate," *IEEE Trans Antennas and Propagation*, vol. 61, no. 10, pp. 5274–5278, Oct 2013.
7. CST Microwave Studio Getting Started Manual, CST Studio Suite 2010.
8. T.A. Milligan, Modern Antenna Design, 2nd Edition, Section 6-6, John Wiley & Sons, Hoboken, New Jersey, 2005.
9. W.-S. Chen, C.-K. Wu, and K.-L. Wong, "Novel Compact Circularly Polarized Square Microstrip Antenna," *IEEE Trans Antennas and Propagation*, vol. 49, no. 3, pp. 340–342, March 2001.
10. P.C. Sharma and K.C. Gupta, "Analysis and Optimized Design of Single Feed Circularly Polarized Microstrip Antennas," *IEEE Trans Antennas and Propagation*, vol. AP-31, no. 6, pp. 949–955, November 1983.
11. R.N. Simons, D. Chun and L.P.B. Katehi, "Microelectromechanical Systems (MEMS) Actuators for Antenna Reconfigurability," 2001 IEEE MTT-S International Microwave Symposium Digest, pp. 215–218, Phoneix, AZ, 20–24 May 2001.
12. R.V. Goteti, R.E. Jackson and R. Ramadoss, "MEMS-Based Frequency Switchable Microstrip Patch Antenna Fabricated Using Printed Circuit Processing Techniques," IEEE Antennas and Wireless Propagation Letters, vol. 5, pp. 228–230, 2006.
13. S.J. Mazlouman, A. Mahanfar, C. Menon and R.G. Vaughan, "A Review of Mechanically Reconfigurable Antennas Using Smart Material Actuators," Proceedings of the 5th European Conference Antennas and Propagation (EUCAP), pp. 1076–1079, Rome, Italy, 11–15 April 2011.
14. Y. Kim, N.-G. Kim, J.-M. Kim, S.H. Lee, Y. Kwon and Y.-K. Kim, "60-GHz Full MEMS Antenna Platform Mechanically Driven by Magnetic Actuator," IEEE Transactions on Industrial Electronics, vol. 58, no. 10, pp. 4830–4836, October 2011.
15. Y. Nada, M. Medhat, M. Nagi, F. Marty, B. Saadany and T. Bourouina, "Mechanical Displacement Multiplier: 250 uM Stable Travel Range MEMS Actuator Using Frictionless Simple Compliant Structures," 2012 IEEE 25th International Conference on Micro Electro Mechanical Systems (MEMS), Paris, France, 29 January–2 February 2011.